

## **Supporting Information**

### **Defective and “*c*-Disordered” *Hortensia*-like Layered MnO<sub>x</sub> as an Efficient Electrocatalyst for Water Oxidation at Neutral pH**

Biaobiao Zhang,<sup>†</sup> Hong Chen,<sup>†</sup> Quentin Daniel,<sup>†</sup> Bertrand Philippe,<sup>‡</sup> Fengshou Yu,<sup>§</sup>  
Mario Valvo,<sup>||</sup> Yuanyuan Li,<sup>⊥</sup> Ram B. Ambre,<sup>†</sup> Peili Zhang,<sup>†</sup> Fei Li,<sup>§</sup> Håkan Rensmo,<sup>‡</sup>  
Licheng Sun<sup>\*,†,§</sup>

<sup>†</sup> Department of Chemistry, KTH Royal Institute of Technology, 10044 Stockholm, Sweden

<sup>‡</sup> Department of Physics and Astronomy, Uppsala University, Box 516, SE-75120, Uppsala, Sweden

<sup>§</sup> State Key Laboratory of Fine Chemicals, Institute of Artificial Photosynthesis, DUT-KTH Joint Education and Research Center on Molecular Devices, Dalian University of Technology (DUT), 116024 Dalian, People's Republic of China

<sup>||</sup> Department of Chemistry - Ångström Laboratory, Uppsala University, Box 538, SE-75121 Uppsala, Sweden

<sup>⊥</sup> Department of Fibre and Polymer Technology, KTH Royal Institute of Technology, 10044 Stockholm, Sweden

*\*Corresponding author Email: [lichengs@kth.se](mailto:lichengs@kth.se)*

## Materials

Ultra pure water ( $18.2 \text{ M}\Omega \cdot \text{cm}^{-1}$ ) for all the reactions or measurements was obtained from a Milli-Q system. All materials were used as received. NaCl (99%),  $\text{Na}_2\text{SO}_4$  (98%),  $\text{KH}_2\text{PO}_4$  (99%),  $\text{K}_2\text{HPO}_4$  (99%),  $\text{D}_2\text{O}$  (99.9%), 40 wt. % KOD in  $\text{D}_2\text{O}$ , 98 atom % D and  $\text{Mn}(\text{CH}_3\text{COO})_2 \cdot 4\text{H}_2\text{O}$  (99%) were purchased from Sigma-Aldrich. Fluorine-doped tin oxide (FTO) substrates were purchased from Pilkington (resistance of  $\sim 8 \text{ }\Omega \cdot \text{cm}^{-2}$ ) and were previously cleaned inside an ultrasonic bath in water and ethanol for 30 min. All other chemicals are commercially available.

## Instruments for structure and surface characterizations

Inductively coupled plasma-optical emission spectroscopy (ICP-OES) was performed on a PerkinElmer Optima 2000 DV instrument. Thermogravimetric and differential Thermogravimetric (TG/DTG) analysis was carried out with a Mettler Toledo TGA/SDTA851 equipment. Soft X-ray Photoelectron spectroscopy (SOXPES) measurements were carried out at the Beamline I-411 at the Swedish National Synchrotron Facility MaxIV Laboratory in Lund, Sweden.<sup>1</sup> The end-station had a wide photon energy range (50 eV to 1500 eV). The pressure in the analysis chamber was  $\sim 10^{-8}$  mbar. A photon energy of 1000 eV (C1s and O1s), 600 eV (P2p) and 400 eV (Mn3s) was used in this work.

Hard X-ray Photoelectron spectroscopy (HAXPES) was carried out at BESSY II (Helmholtz Zentrum Berlin, Germany) at the KMC-1 beamline<sup>2</sup> using the HIKE end-station.<sup>3</sup> An overview is presented and was recorded with a photon energy of 2500 eV. The pressure in the analysis chamber was  $\sim 10^{-8}$  mbar during measurement. All the spectra presented were energy calibrated by setting the adventitious carbon peak to 285 eV binding energy. The peak positions and areas were optimized by a weighted least-squares fitting method using CasaXPS software. Charging and beam damage were

controlled by following peak positions and peak shape with variations in light intensity and time. No changes were observed in the spectra reported here. The quantification presented are based on the measurements recorded at 2500 eV and calculated from the experimental results after correcting the intensity by the photoionization cross section for each element at their specific photon energy, using database values.<sup>4</sup> The peak fitting of the Mn3s core levels presented in this work were based on reference investigated in a previous work (ref 43). The FWHM of the fitting peaks was fixed as well as the  $\Delta E_{3s}$ , i.e. the peaks presented show the peak expected for pure  $Mn^{x+}$  phases (4.4 for  $Mn^{4+}$ , 5.7 for  $Mn^{3+}$  and 6.3 for  $Mn^{2+}$ ). The minimum number of peaks was then introduced to fit the spectra highlighting the main oxidation present regarding Mn.

Raman spectroscopy was performed via a Renishaw inVia Raman spectrometer with a laser wavelength of 532 nm. A 50 $\times$  magnification objective and a nominal power of 0.5 mW were utilized for the analyses. A preliminary calibration was run on a Si wafer to have a characteristic reference peak at 520.6  $cm^{-1}$ . Sixty acquisitions with a measuring time of 30 s were taken for each spectrum to improve the signal-to-noise ratio. Beam exposure between subsequent scans was minimized to prevent possible degradation of the samples. Scanning electron microscopy (SEM) images were obtained by using a Nova NanoSEM 450 equipment. Images were obtained with an acceleration voltage of 3 kV. Energy dispersive X-ray (EDX) elemental maps were obtained on a Hitachi S-4800 with an acceleration voltage of 15 kV. Atomic force microscope (AFM) investigation was performed by using Bruker MultiMode 8 AFM in "tapping" mode. The attenuated total reflectance Fourier transform infrared spectroscopy (ATR-FTIR) spectra were measured on a Thermo Scientific Nicolet Is5 FT-IR spectrometer. X-ray diffraction (XRD) measurements were carried out on Panalytic X'pert PRO XRD diffractometer with Cu  $K\alpha$  radiation. TEM images and selected area diffraction (SAED) were taken on a JEOL JEM2100F transmission electron microscope.

## Film Preparation

In a typical experiment, a three-electrode cell equipped with FTO electrode (effective area  $2 \times 1 \text{ cm}^2$ ) as working electrode, a platinum mesh ( $1 \times 2 \text{ cm}^2$ ) as counter electrode and an Ag/AgCl aqueous KCl (3.5 M) reference electrode was used for electro-deposition at 1.4 V in a aqueous solution of 5 mM  $(\text{CH}_3\text{COO})_2\text{Mn}$  and 50 mM NaCl for 30 minutes. The formed brown films were then rinsed thoroughly with demineralized water and dried under air at room temperature ( $\text{MnO}_x$ -as). Further heating at 300 °C for 2 hours was performed in order to obtain the active  $\text{MnO}_x$ -300.

## Electrochemical measurements

All electrochemical experiments employed a CHI 650e potentiostat in a single-compartment cell with three-electrode configuration. The cell was equipped with a FTO electrode with manganese oxide film as the working electrode ( $0.5 \times 0.5 \text{ cm}^2$ ), a platinum mesh ( $1 \times 2 \text{ cm}^2$ ) as the counter electrode and an Ag/AgCl (3.5 M KCl in water) reference electrode. All experiments were conducted at ambient temperature ( $\sim 23^\circ\text{C}$ ). All linear scan voltammograms (LSV) were measured with a scan rate of  $10 \text{ mV s}^{-1}$ . The activities of manganese oxides were evaluated both with and without 95% iR correction. For each test, there is a caption to clarify that the test was performed with or without iR correction. Tafel plots were measured with stirring to remove mass transport limitations.<sup>5</sup> Potentials were converted to NHE scale by the following relation,  $E_{\text{NHE}} = E_{\text{Ag/AgCl}} + 0.197 \text{ V}$ . Overpotentials ( $\eta$ ) for the oxygen evolution reaction from water were calculated by  $\eta = E_{\text{NHE}} - 0.82 \text{ V}$ .

Electrochemical impedance spectroscopy (EIS) was carried out in 1.0 M KPi in a three-electrode configuration, the frequency ranged from  $0.1\text{--}10^5 \text{ Hz}$  with an applied AC amplitude of 1.25 V.

To determine the Faradaic efficiency, the cell was sealed and purged with Argon. The electrolysis was carried out with a constant potential at 1.4 V, and the actual quantity of O<sub>2</sub> evolution was determined by gas chromatography every 30 min. The theoretical amount of produced oxygen can be obtained by converting the charge passed to  $\mu\text{mol}$  gas according to Faraday's Law. The Faradaic efficiency was calculated as  $\text{O}_2(\text{actual})/\text{O}_2(\text{theoretical}) \times 100\%$ .

### **Determination of the average manganese oxidation state by redox titration**

The method followed an established procedure for the quantification of MnO<sub>2</sub>.<sup>6,7</sup> MnO<sub>x</sub>-300: Carefully weighed sample of MnO<sub>x</sub>-300 (3.9 mg) was mixed with a solution of sodium oxalate (1.0 mL, 0.2 M) and sulfuric acid (1.0 mL, 0.5 M). The solution was stirred at 60°C until all oxide had dissolved and a brown solution formed. In this step manganese is quantitatively reduced to Mn<sup>2+</sup> solution. In the following, the excess of oxalate was determined by titration at around 60°C with 0.04 M KMnO<sub>4</sub> (1.65 ml KMnO<sub>4</sub> solution was consumed).

MnO<sub>x</sub>-as: Carefully weighed sample of MnO<sub>x</sub>-as (4.4 mg) was mixed with a solution of sodium oxalate (1.0 mL, 0.2 M) and sulfuric acid (1.0 mL, 0.5 M). The solution was stirred at 60°C until all oxide had dissolved and a brown solution formed. In this step manganese is quantitatively reduced to Mn<sup>2+</sup> solution. In the following, the excess of oxalate was determined by titration at around 60°C with 0.04 M KMnO<sub>4</sub> (1.63 ml KMnO<sub>4</sub> solution was consumed).

In combination with the manganese content of the material (determined by ICP-AES, weight% of Mn 55% for MnO<sub>x</sub>-300 and 49% for MnO<sub>x</sub>-as), the average oxidation state of the manganese centres could then be calculated by the following equation:

$$\text{Average oxidation state} = \frac{2 \times n_{\text{oxalate}} - 5 \times n_{\text{consumed KMnO}_4}}{n_{\text{Mn}}} + 2 \quad (1)$$

Finally, the average Mn oxidation states of 3.9 and 3.8 are obtained for MnO<sub>x</sub>-as and MnO<sub>x</sub>-300, respectively.

### Electrochemical active surface area

To measure electrochemical capacitance, the potential was swept between a small potential range at different scan rates. The cyclic voltammograms can be seen in Figure 2d and S15. We measured the capacitive currents in a potential range where no faradic processes are observed, i.e. at 0.94 V *vs.* NHE for MnO<sub>x</sub>-300 and at 0.87 V *vs.* NHE for MnO<sub>x</sub>-as. The measured capacitive currents are plotted as a function of the scan rate in the insets of Figure 2d and S17, and a linear fit determined the specific capacitance to be 40.0 mF·cm<sup>-2</sup> for MnO<sub>x</sub>-300 and 39.4 mF·cm<sup>-2</sup> for MnO<sub>x</sub>-as. The specific capacitance can be converted into an electrochemical active surface area (ECSA) using the specific capacitance value for a flat standard with 1.0 cm<sup>2</sup> of real surface area. The specific capacitance for a flat surface is generally found to be in the range of 20-60 μF·cm<sup>-2</sup>. For surface area calculations in this work we assume a middle value of 40 μF·cm<sup>-2</sup>.

$$ECSA_{MnO_x-300} = \frac{40.0 \text{ mF} \cdot \text{cm}^{-2}}{40.0 \text{ } \mu\text{F} \cdot \text{cm}^{-2} \text{ per cm}^2_{ECSA}} = 1000 \text{ cm}^2 \quad (2)$$

$$ECSA_{MnO_x-as} = \frac{39.4 \text{ mF} \cdot \text{cm}^{-2}}{40.0 \text{ } \mu\text{F} \cdot \text{cm}^{-2} \text{ per cm}^2_{ECSA}} = 985 \text{ cm}^2 \quad (3)$$

### Calculation of mass activity and TOF

The average loading of manganese oxide was obtained by scraping the samples down from the FTO surface and then weighing by a Mettler Toledo micro balance (accuracy 0.01 mg). 20 MnO<sub>x</sub>-300 electrodes (2×1 cm<sup>2</sup>) with a total size of 40 cm<sup>2</sup> were prepared and scraped. The total weight of the scraped manganese oxide powder is 4.8 mg, therefore the calculated average amount of the manganese oxide is 0.12 mg·cm<sup>-2</sup>, and consequently results in a Mn atom amount of 1.2 μmol·cm<sup>-2</sup>. The mass activity and TOF can be calculated by the following equation:

$$\text{Mass activity} = \frac{j}{M} \quad (4)$$

$$\text{TOF} = \frac{jA}{4nF} \quad (5)$$

Where  $j$  is the current density in  $\text{A}\cdot\text{cm}^{-2}$ , while  $M$  is the mass of the catalyst loading ( $\text{g}\cdot\text{cm}^{-2}$ ),  $A$  is the working electrode area ( $\text{cm}^2$ ),  $n$  is the number of moles of the loaded catalyst ( $\text{mol}\cdot\text{cm}^{-2}$ ), and  $F$  is the Faraday constant ( $\text{C}\cdot\text{mol}^{-1}$ ).

### **Probing the presence of $\text{Mn}^{3+}$ in the $\text{MnO}_x$ -300 film**

Electronic absorption spectra were measured with a PerkinElmer Lambda 750 UV-Vis spectrophotometer. For the detection of  $\text{Mn}^{3+}$  on the surface of  $\text{MnO}_x$ -300, 3.0 ml 20 mM pyrophosphate solution containing 1.0 M KPi electrolyte was used as a spectral reference. Then a  $1\times 1\text{ cm}^2$   $\text{MnO}_x$ -300 or  $\text{MnO}_x$ -as films were dipped into the above solution for 5 min, followed by testing the UV-Vis absorption of this solution.

### **In-situ UV-Vis Spectroscopy**

The thin  $\text{MnO}_x$  films for in-situ UV-Vis study were electrodeposited at 1.4 V in a aqueous solution of 5 mM  $(\text{CH}_3\text{COO})_2\text{Mn}$  and 50 mM NaCl for 25 s and then followed by an annealing at 300 degree. LSV curve of this thin  $\text{MnO}_x$ -300 shows the same onset potential for water oxidation as normal  $\text{MnO}_x$ -300 (Figure S24), indicating that the obtained thin  $\text{MnO}_x$ -300 film is the same species as the  $\text{MnO}_x$ -300 prepared under the previous conditions in this work. Electronic absorption spectra under different potentials were measured with a PerkinElmer Lambda 750 UV-vis spectrophotometer.

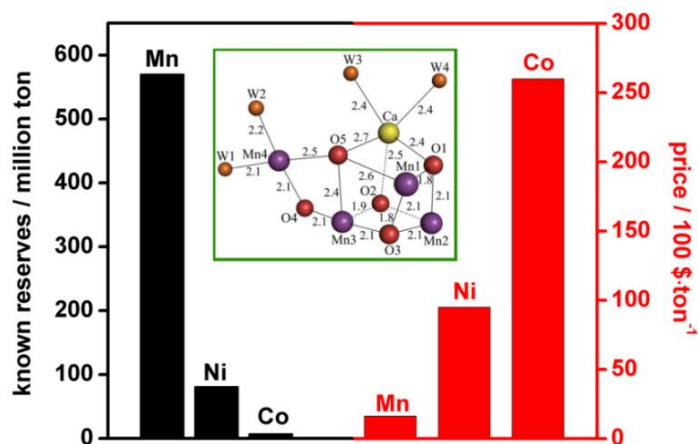


Figure S1. Known global reserves and prices of Mn, Ni and Co. The inset represents the structure of the  $\text{Mn}_4\text{CaO}_5$  cluster in PSII in the dark-stable  $S_1$ -state.<sup>8</sup>

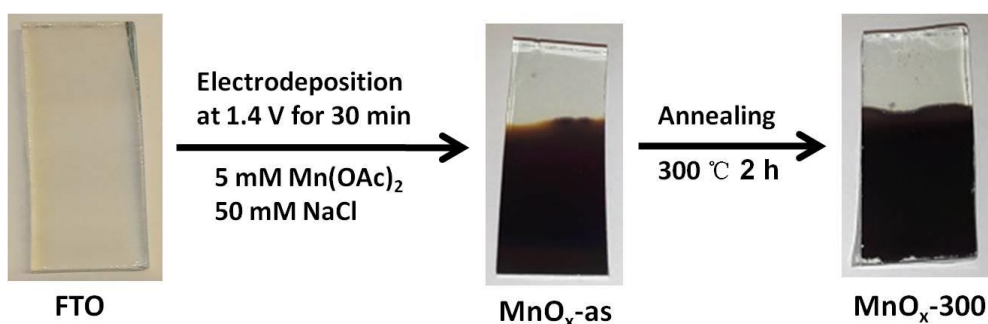


Figure S2. Preparation of  $\text{MnO}_x\text{-as}$  and  $\text{MnO}_x\text{-300}$ .

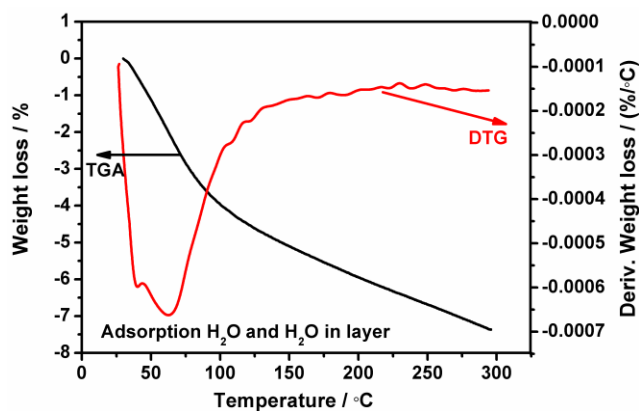


Figure S3. TG/DTG analysis of  $\text{MnO}_x\text{-300}$ .

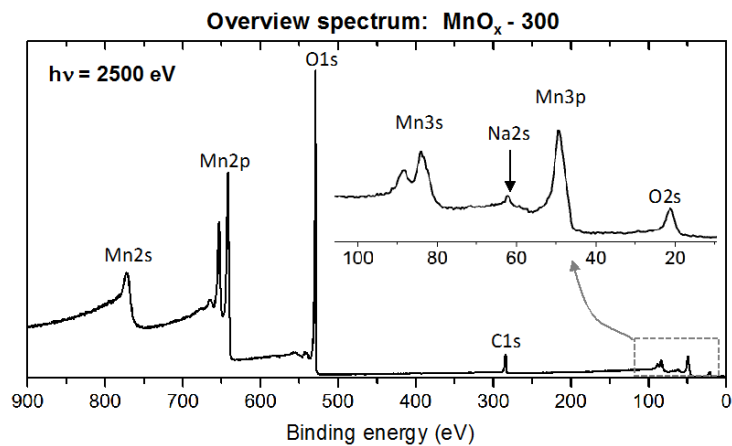


Figure S4. Overview XPS spectrum of the MnO<sub>x</sub>-300 deposited on FTO sample recorded by HAXPES with a photon energy of 2500 eV. The inset presents an enlargement of the low binding energy area.

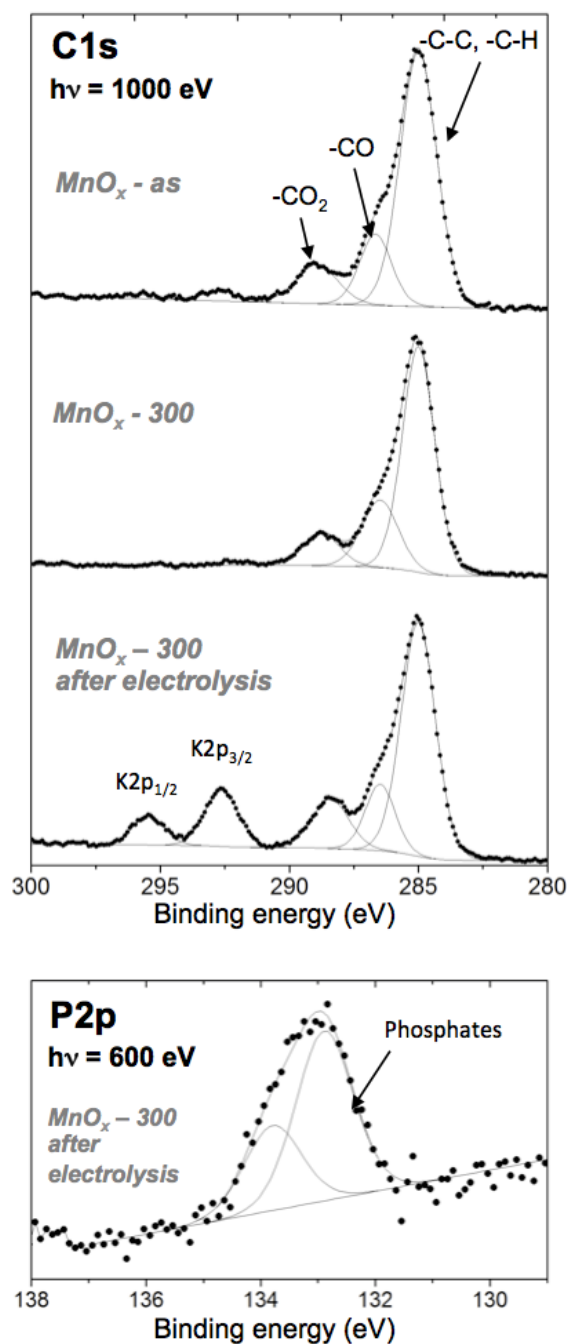


Figure S5. (Top) C1s core level peaks spectra (SOXPES,  $h\nu = 1000 \text{ eV}$ ) of  $\text{MnO}_x$ -as,  $\text{MnO}_x$ -300 and  $\text{MnO}_x$ -300 after electrolysis in 1.0 M pH 7.0 KPi solution at 1.4 V without iR correction for 30 min. (Bottom) P2p core level peak spectrum of  $\text{MnO}_x - 300$  after electrolysis recorded with a photon energy of 600 eV.

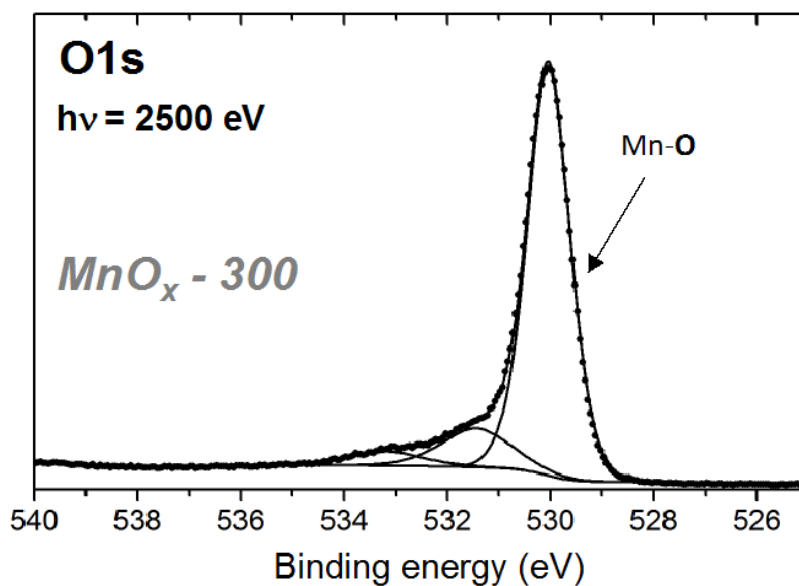


Figure S6. O1s core level peak spectrum of  $\text{MnO}_x$ -300 recorded with a photon energy of 2500 eV.

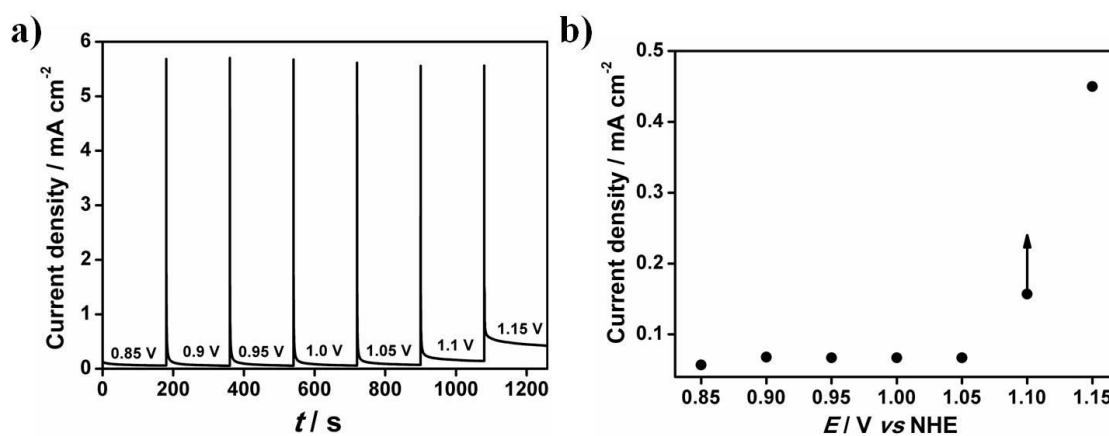


Figure S7. a) Multi-potential-step chronoamperometry of  $\text{MnO}_x$ -300 in 1.0 M pH 7.0 KPi solution with a potential step of 0.05 V; b) current density plots under different potential steps.

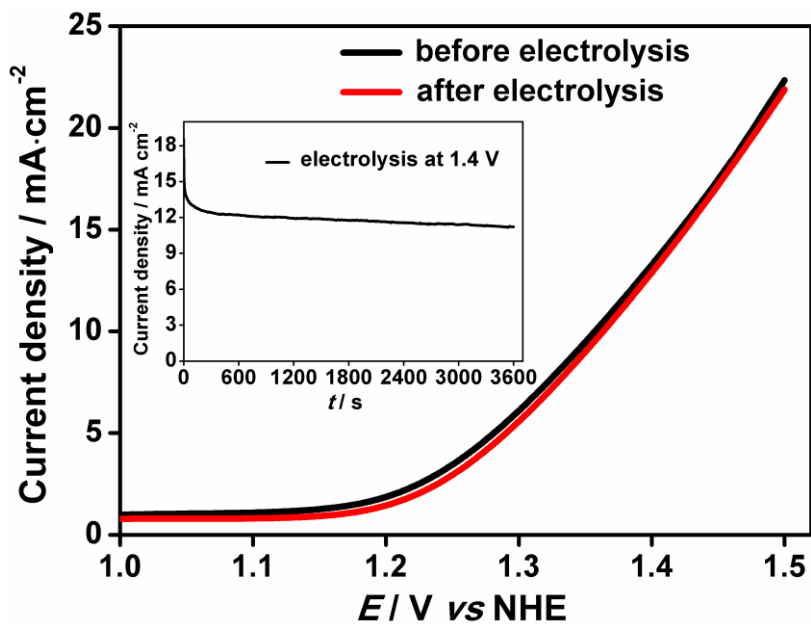


Figure S8. LSV curves of  $\text{MnO}_x\text{-300}$  before (black) and after (red) electrolysis at 1.4 V for 1.0 h. The inset presents the bulk electrolysis curves. The LSV scan rate is 10 mV/s. All experiments were carried out in 1.0 M pH 7.0 KPi solution without iR correction.

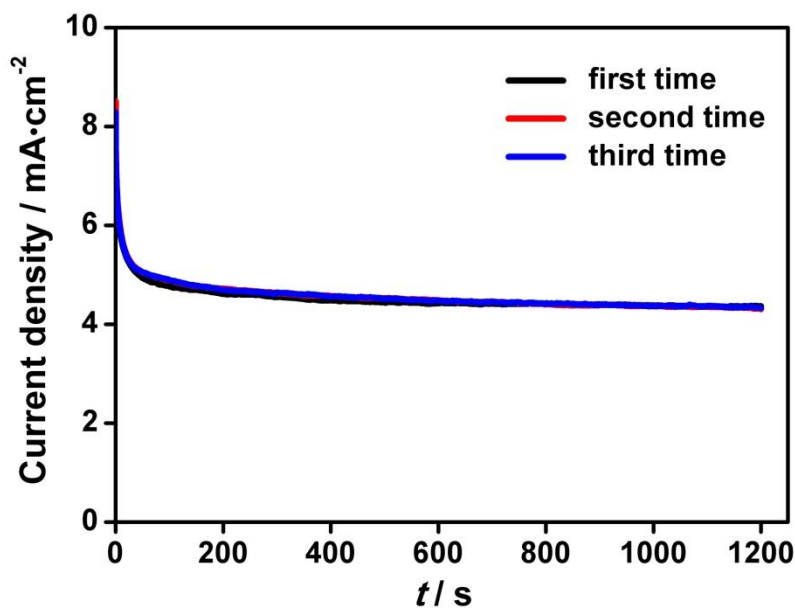


Figure S9. Repetition of bulk electrolysis of  $\text{MnO}_x\text{-300}$  at 1.3 V in 1.0 M pH 7.0 KPi solution without iR correction for 20 min.

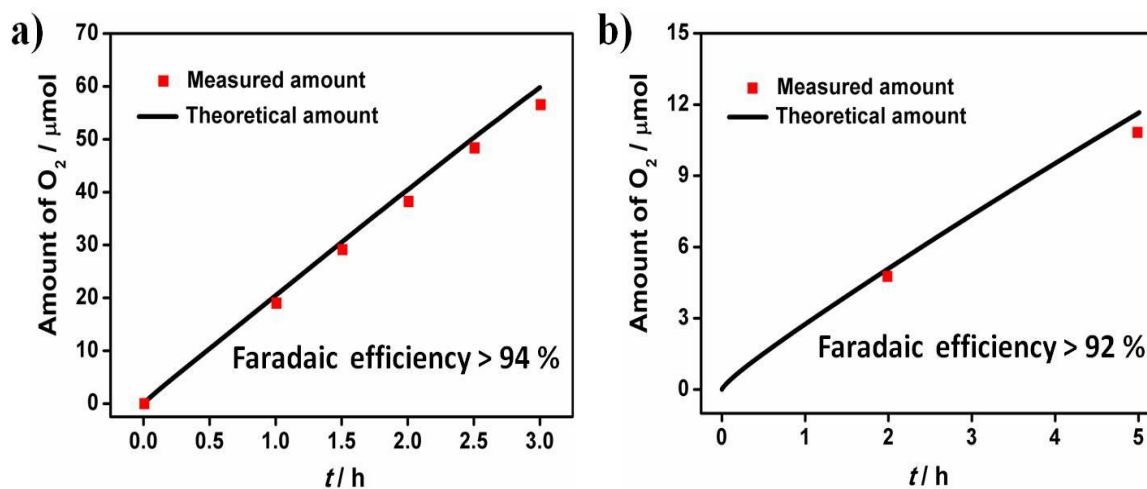


Figure S10. Faradaic efficiency. The experimental and theoretical  $O_2$  evolution amount by electrolysis of  $MnO_x$ -300 in 1.0 M pH 7.0 KPi solution at a) 1.4 V b) 1.16 V without iR correction.

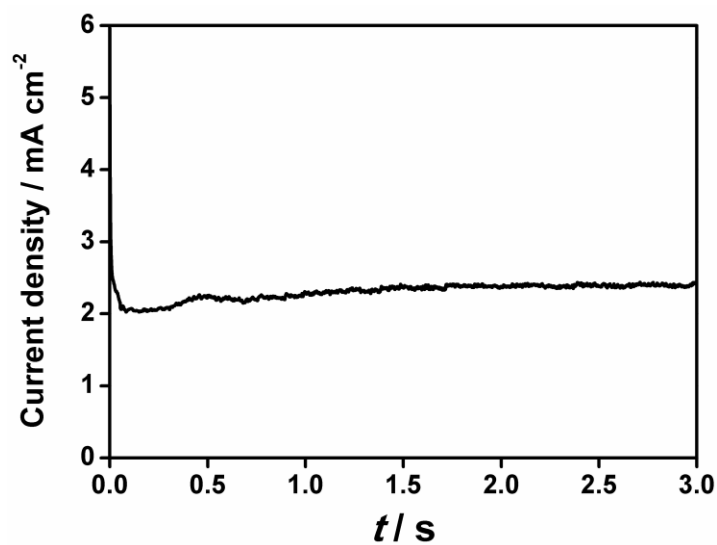


Figure S11. Controlled-potential electrolysis of  $MnO_x$ -300 at 1.3 V for 3 h in 0.1 M pH 7.0 KPi solution without iR correction.

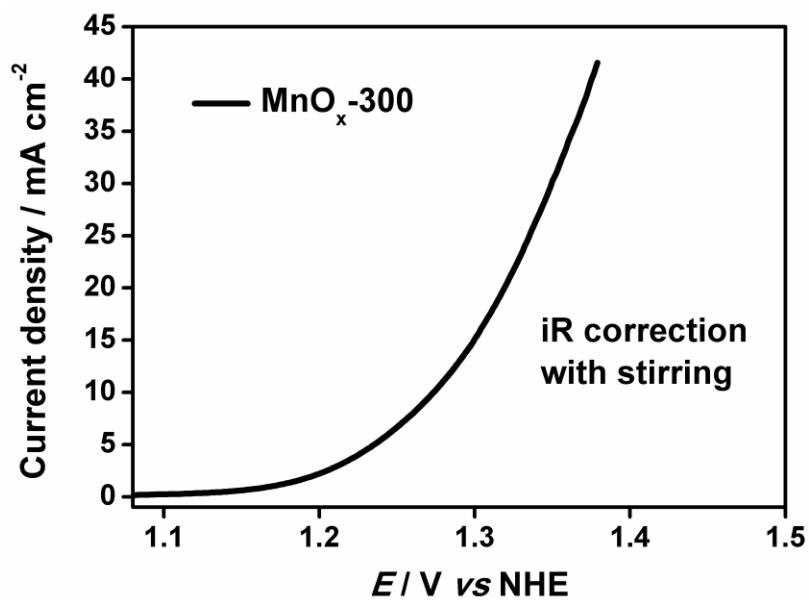


Figure S12. LSV curve of  $\text{MnO}_x\text{-300}$  in 1.0 M KPi buffer electrolyte with scan rate 10 mV/s, 95% iR correction and stirring.

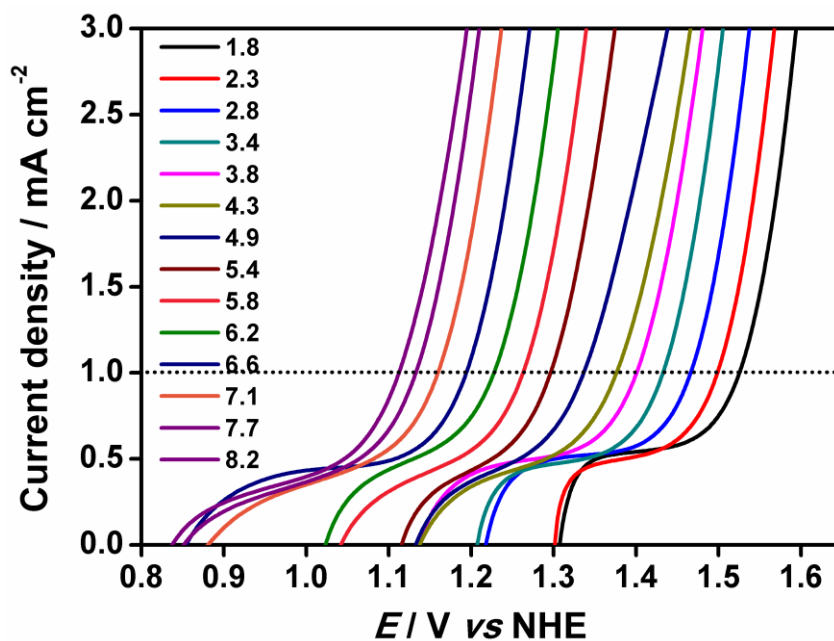


Figure S13. LSV curves of  $\text{MnO}_x\text{-300}$  in 1.0 M KPi buffer electrolyte of various pH values with scan rate 10 mV/s, no iR correction.

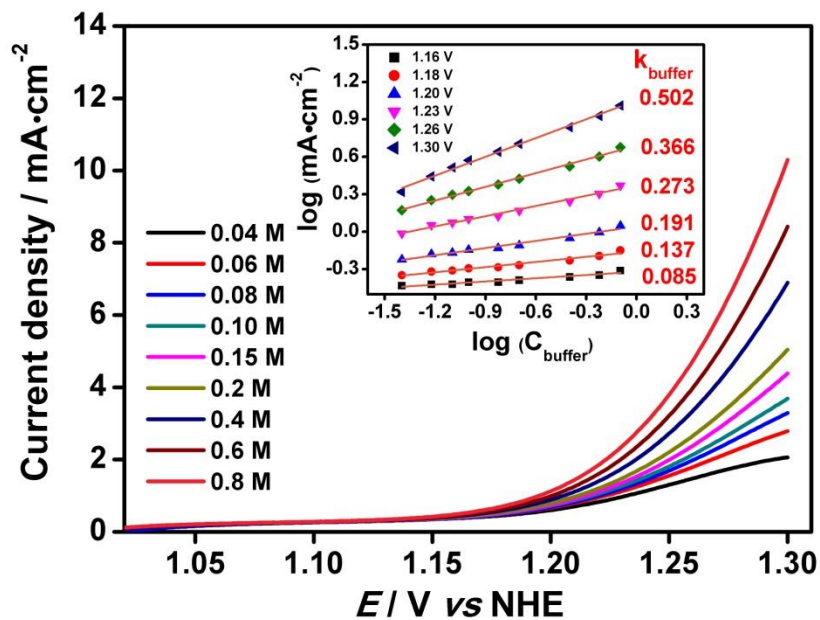


Figure S14. LSV curves of MnO<sub>x</sub>-300 in different concentration of KPi buffer electrolyte with scan rate 10 mV/s and 95% iR correction. The inset presents the KPi buffer concentration dependence of the catalytic current density at various potential. The values of k<sub>buffer</sub> were obtained from the slope of each fitting curve.

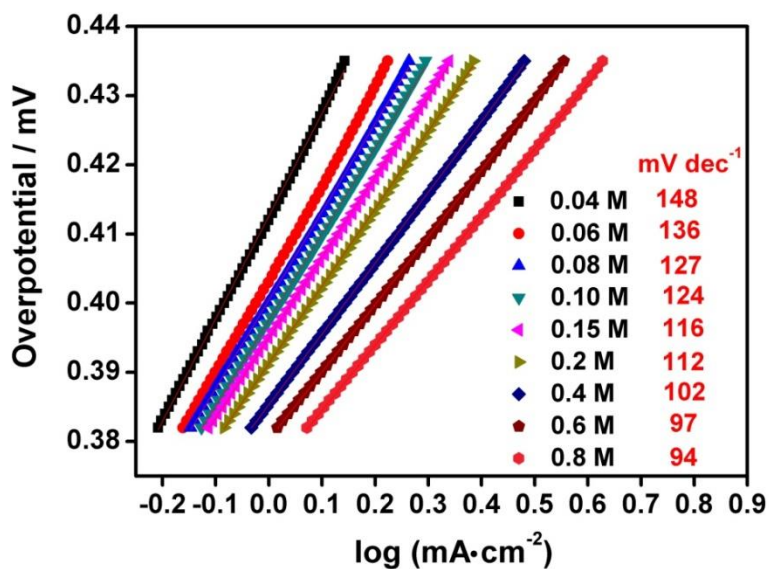


Figure S15. Tafel plots of MnO<sub>x</sub>-300 film in different concentrations of KPi buffer electrolyte.

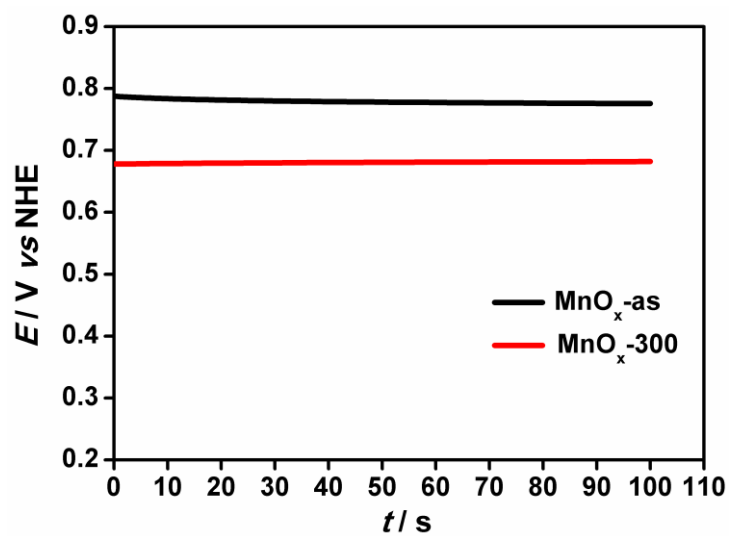


Figure S16. OCP curves of MnO<sub>x</sub>-as (black) and MnO<sub>x</sub>-300 (red) in 1.0 M pH 7.0 KPi solution.

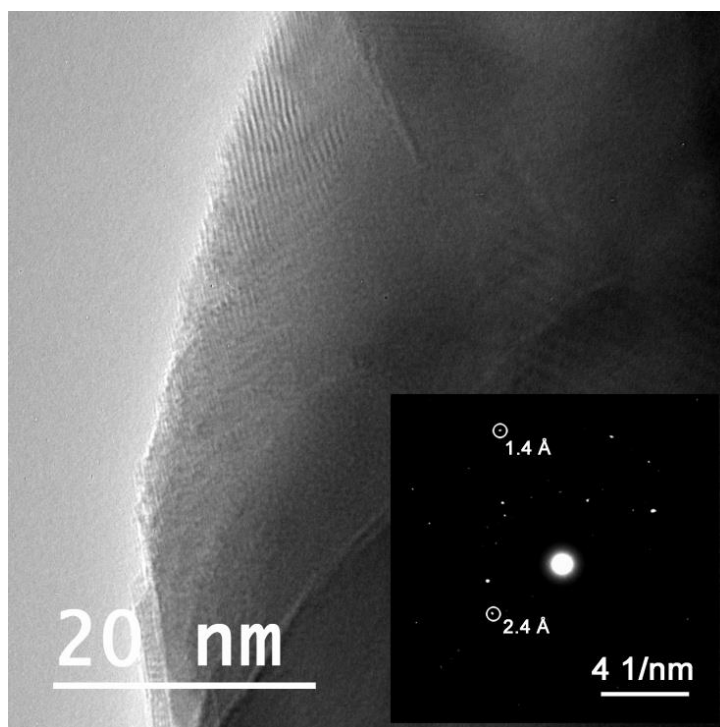


Figure S17. TEM image of MnO<sub>x</sub>-as, the inset presents the associated SAED.

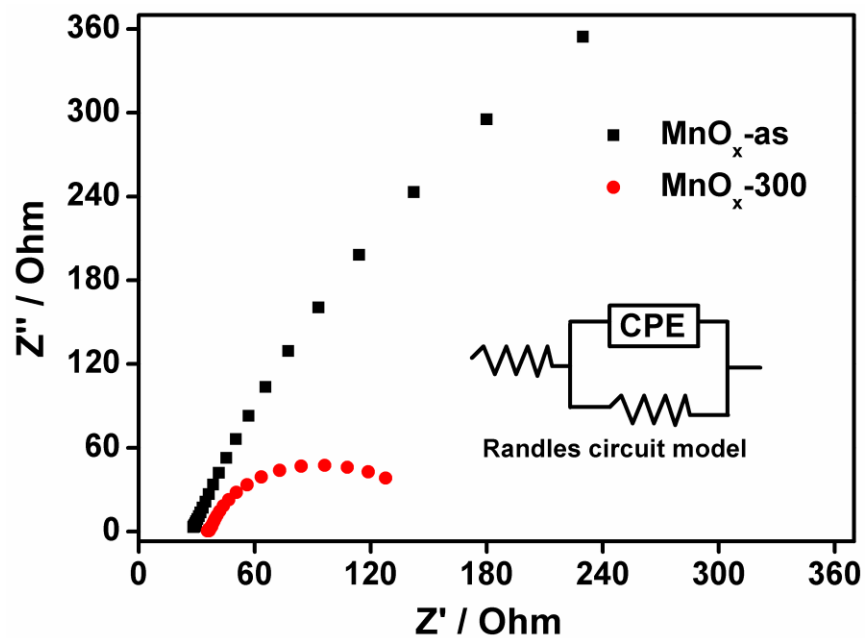


Figure S18. Nyquist diagram of  $\text{MnO}_x\text{-300}$  and  $\text{MnO}_x\text{-as}$ .

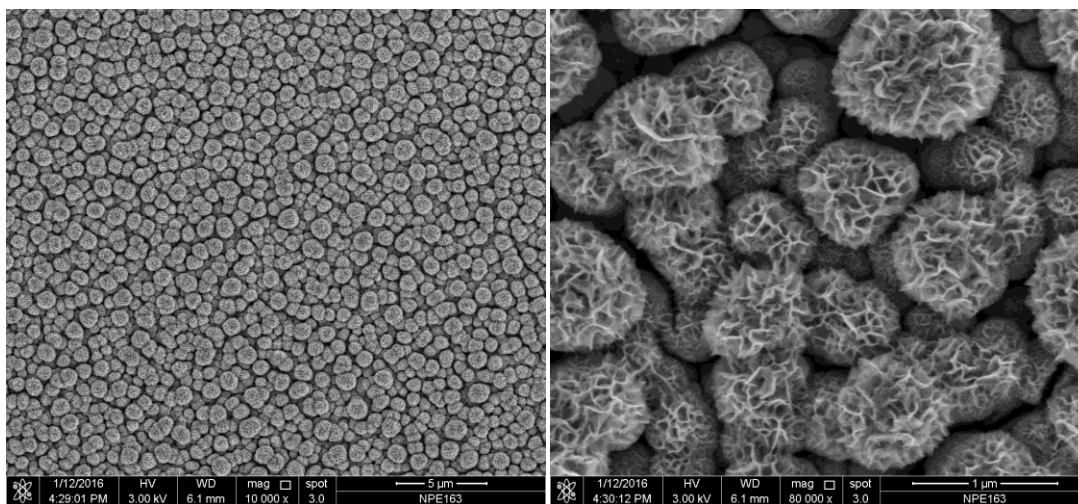


Figure S19. SEM images of  $\text{MnO}_x\text{-as}$  taken at different magnifications. Note the Hortensia-like morphology of the deposits in the magnified micrograph.

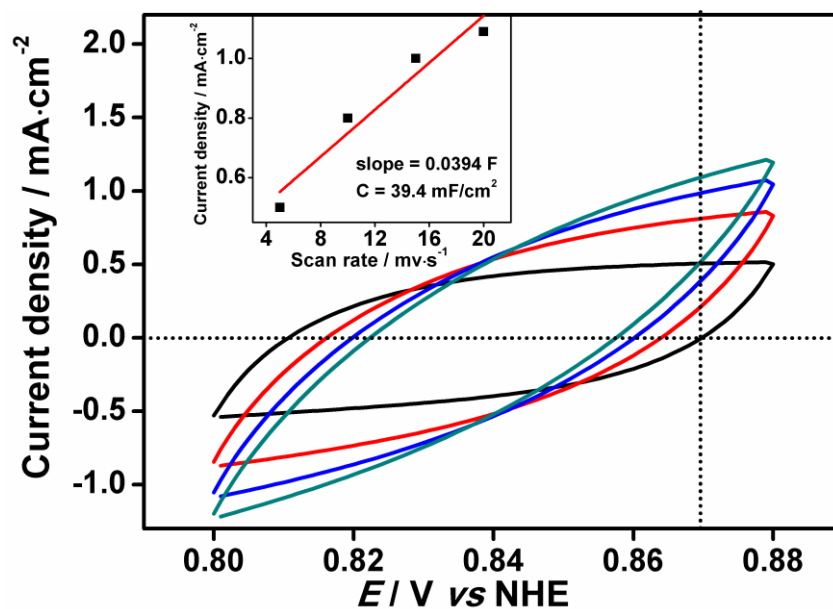


Figure S20. Electrochemical capacitance measurements for determining the ECSA of the  $\text{MnO}_x$ -as film. The inset shows the measured capacitive currents plotted as a function of the scan rate.

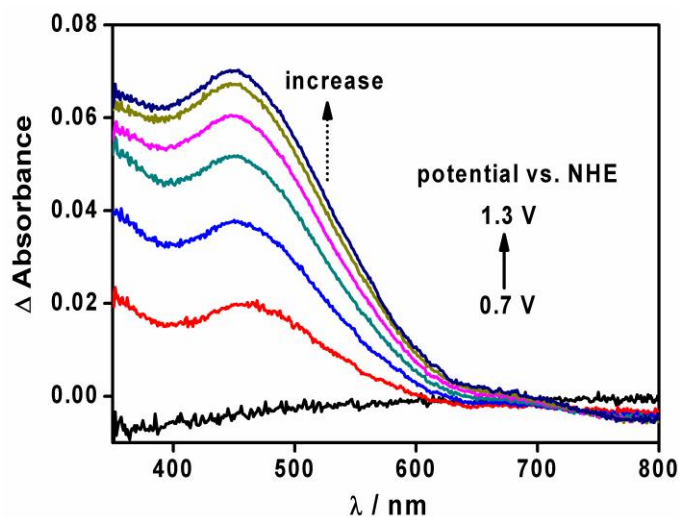


Figure S21. The changes in the UV-Vis absorption of the thin  $\text{MnO}_x$ -as film measured at increasing potential from 0.7 V to 1.3 V with a 0.1 V increment.

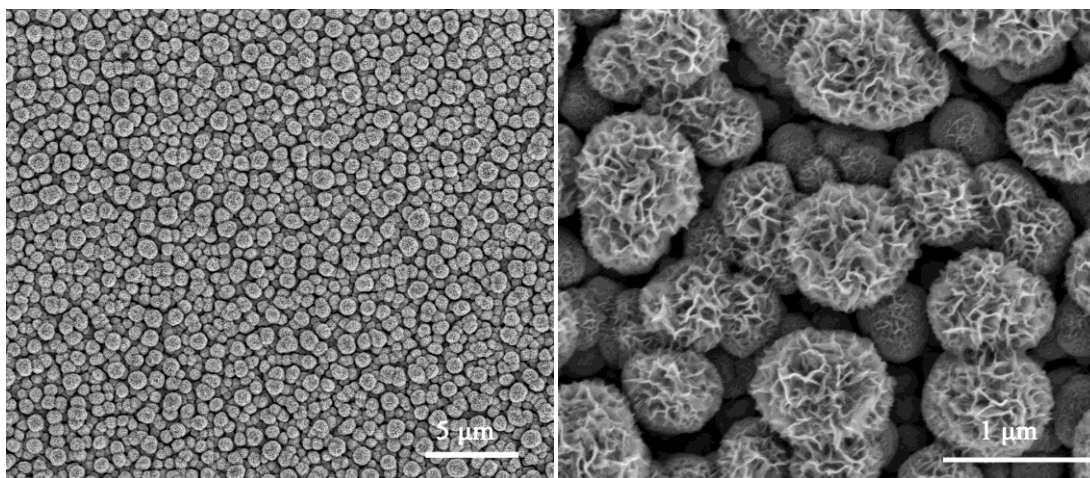


Figure S22. SEM images of  $\text{MnO}_x$ -300 after electrolysis in 1.0 M pH 7.0 KPi solution at 1.4 V without iR correction for 30 min. Note that the initial Hortensia-like morphology is fully retained after the electrolysis process.

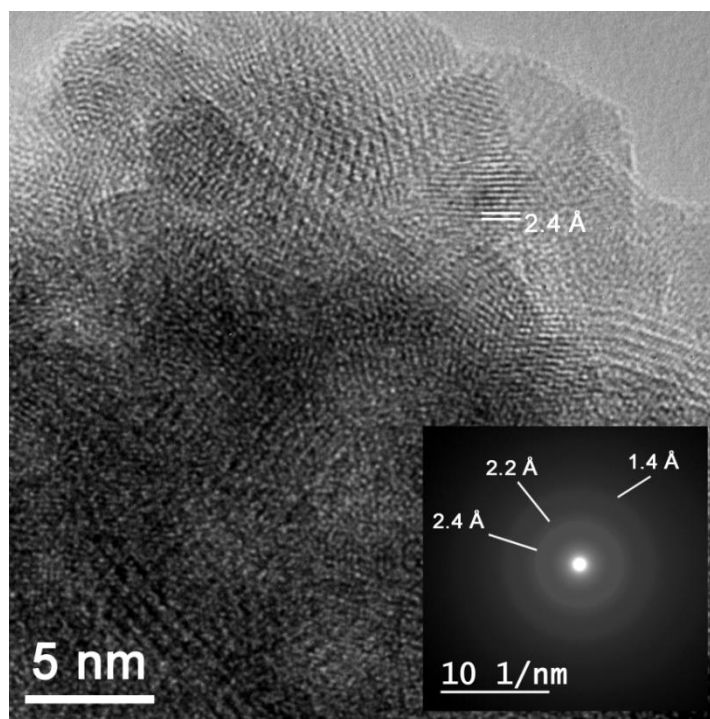


Figure S23. HRTEM image of  $\text{MnO}_x$ -300 after electrolysis in 1.0 M pH 7.0 KPi solution at 1.4 V without iR correction for 30 min. The inset displays the correspondent SAED where only diffused diffraction rings can be noticed.

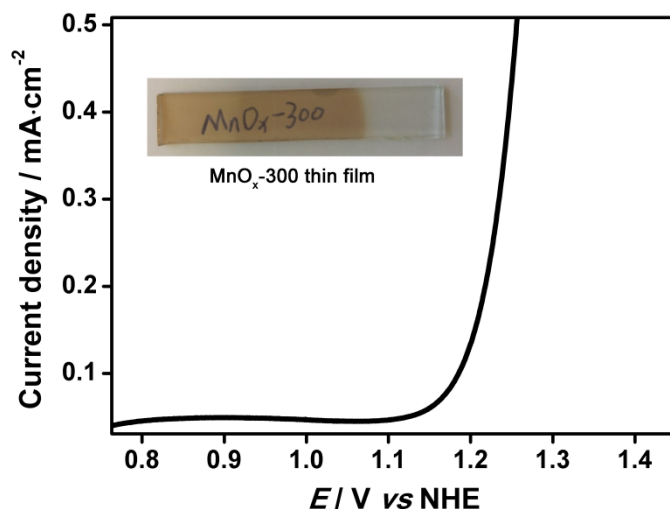


Figure S24. LSV curve of  $\text{MnO}_x$ -300 thin film at scan rate of 10 mV/s in 1.0 M pH 7.0 KPi solution without iR correction.

## References

- (1) Bässler, M.; Forsell, J.-O.; Björneholm, O.; Feifel, R.; Jurvansuu, M.; Aksela, S.; Sundin, S.; Sorensen, S. L.; Nyholm, R.; Ausmees, A.; Svensson, S. *J. Electron Spectros. Relat. Phenomena* **1999**, 101-103, 953-957.
- (2) Schaefer, F.; Mertin, M.; Gorgoi, M. *Rev. Sci. Instrum.* **2007**, 78, 123102.
- (3) Gorgoi, M.; Svensson, S.; Schäfers, F.; Öhrwall, G.; Mertin, M.; Bressler, P.; Karis, O.; Siegbahn, H.; Sandell, A.; Rensmo, H.; Doherty, W.; Jung, C.; Braun, W.; Eberhardt, W. *Nucl. Instrum. Methods Phys. Res. A* **2009**, 601, 48-53.
- (4) Yeh, J. J.; Lindau, I. *At. Data Nucl. Data Tables* **1985**, 32, 1-155.
- (5) Huynh, M.; Bediako, D. K.; Nocera, D. G. *J. Am. Chem. Soc.* **2014**, 136, 6002-6010.
- (6) Wiechen, M.; Zaharieva, I.; Dau, H.; Kurz, P. *Chem. Sci.* **2012**, 3, 2330-2339.
- (7) Frey, C. E.; Wiechen, M.; Kurz, P. *Dalton Trans.* **2014**, 43, 4370-4379.
- (8) Umena, Y.; Kawakami, K.; Shen, J. R.; Kamiya, N. *Nature* **2011**, 473, 55-60.